Canadian Science Publishing

ARTICLE

Evaluation of the internal blast resistance of a bi-directionally prestressed concrete tubular structure according to ANFO explosive charge weight

Ji-Hun Choi, Seung-Jai Choi, Tae-Hee Lee, Dal-Hun Yang, and Jang-Ho Jay Kim

Abstract: When an extreme internal loading is applied to prestressed concrete (PSC) structures, serious property damage and human casualties may occur. However, the existing designs for PSC structures such as prestressed concrete containment vessels (PCCVs) do not include features to protect the structure from forces such as explosive blasts. Therefore, we evaluated the internal blast-resistance of PSC structures using blast tests on bi-directionally prestressed tubular concrete members. The goal of the study was to examine structural behavior data after an internal detonation. Explosive charges (ammonium nitrate – fuel oil; ANFO) were detonated at the center of the mid-span of the concrete tube with a standoff distance of 1000 mm. The data acquired included blast pressure, deflection, strain, crack pattern, and prestressing loss. The data were used to calculate the internal blast charge weight required to cause a PCCV to fail and to calibrate a simulation program to be used commercially for internal blast simulations at real scale structure.

Key words: internal blast, prestressed concrete, PCCV, explicit finite element.

Résumé : Lorsque des charges extrêmes provenant d'une explosion interne sont appliquées à des structures en béton précontraint (BP), des dommages matériels graves et des pertes humaines peuvent survenir. Toutefois, les conceptions actuelles des structures de BP, comme les enceintes de confinement en béton précontraint (ECBP), ne comprennent pas de dispositifs pour protéger la structure contre les explosions. Par conséquent, la capacité de résistance des structures en BP aux explosions internes a été évaluée par des essais d'explosion interne sur des éléments tubulaires BP bidirectionnels. L'objectif de l'étude était d'obtenir les données sur le comportement structurel provenant d'une détonation interne. Les charges de l'ANFO ont été déclenchées au centre de la mi-portée de l'échantillon tubulaire avec une distance de sécurité de 1000 mm. Les données acquises comprenaient la pression de l'explosion, la déflexion, la déformation, le profil de fissure et la perte de précontrainte. Les données ont été utilisées pour dériver les équations afin de calculer le poids de charge interne requis pour faire faillir une ECBP réelle et pour étalonner un programme de simulation commerciale à utiliser pour les simulations d'explosions internes. [Traduit par la Rédaction]

Mots-clés : explosion interne, béton précontraint, enceintes de confinement en béton précontraint (ECBP), élément fini explicite.

Introduction

Prestressed concrete containment vessels (PCCVs) are built as bi-directional prestressed concrete (PSC) structures. They have improved stiffness and strength compared with reinforced concrete (RC); however, PSC is relatively brittle, and when an instantaneous extreme blast load is applied to a PSC member, it fails catastrophically with a sudden loss of load-bearing capacity. Because of this, tests and simulations are performed to analyze the structural stiffness and strength of a concrete member under extreme loading. Because of the difficulties associated with conducting blast tests in the field as well as precise blast simulations, only a small number of studies on extreme loading of PSC structures have been performed. However, because of current worldwide concerns about terrorism and accidents, accurate predictions of structural resistance to blast loading are urgently needed. Among the various types of blasts that can affect structures or infrastructure, the most dangerous is an internal blast that can continuously reflect blast waves inside an enclosed space. However, measuring internal blast pressure is very difficult because pressure gauges installed inside an enclosed space will be damaged by the blast. For this reason, there are no data available on the effects of internal blasts on structural members.

Despite the technological advances in the design and construction of nuclear power plants current code requirements do not consider extreme scenarios such as blasts or collisions within nuclear power plants (Choi et al. 2018). The public assumes that PCCVs are relatively safe from blasts, impacts, or other accidents; however, several disasters such as happened in Chernobyl (Russia) in 1986 and Fukushima (Japan) in 2011, revealed that PCCVs are vulnerable to extreme disaster scenarios. Thus, in-depth studies of PCCVs that rely on accurate damage assessments and safety evaluations are needed. Therefore, in this study, a scaled-down model of a PCCV was designed and fabricated to test and analyze internal blast resistance.

Received 21 October 2019. Accepted 9 August 2020.

J.-H. Choi, S.-J. Choi, T.-H. Lee, D.-H. Yang, and J.-H.J. Kim. School of Civil and Environmental Engineering, Yonsei University, 50 Yonsei-Ro, Seodaemun-Gu, Seoul 03722, Republic of Korea.

Corresponding author: Jang-Ho Jay Kim (email: jjhkim@yonsei.ac.kr).

Internal blast loading theory

Using the results from our literature review of strategies to prevent disasters in PCCVs, we focused on field studies for evaluating the safety and structural integrity of seismic and static internal pressure loading. Recently, a limited number of studies on external blast and aircraft impact scenarios were performed that included disaster prevention for the structures. For critical infrastructure such as PCCVs and storage tanks for liquid natural gas, disaster prevention and blast protection against extreme loading must be incorporated at the design stage. The damage or collapse of such structures can lead to insurmountable environmental problems and human casualties. However, due to test facility limitations and overall cost burden, much of the research is restricted to analytical methods and computer simulations where the reliability of the findings is questionable.

Only a handful of studies have focused on the effects from external blasts and low-velocity impacts on structural concrete members (Choi et al. 2018; Yi et al. 2012). The only meaningful experimental study to date on internal loading of a PCCV was performed at the Sandia National Laboratory in the USA. In that study, they conducted an experiment to study the scaling effect of steel containment vessels and PCCV behavior under extreme quasi-static internal pressure buildup (Hessheimer et al. 2003). Cost and testing site restrictions, however, make it nearly impossible to conduct internal blast tests. For this reason, almost no internal blast studies have been conducted, thus, this study investigated the damage from internal blast loading in a PSC tubular member. To determine the effect of varying the explosive pressure on a structural member, the study focused on the weight of the explosive charge as the independent variable and the structural behavior as the dependent variable.

Materials and methods

Blast-experiment modeling

Internal blast loading characteristics and scenario

Blast loading is classified as either restrained or unrestrained based on whether it is an external or internal explosion, respectively. A restrained blast generates greater pressure than a unrestrained blast because of the confinement. When direct blast pressure reaches the inner surface of a structure, a free-field incident and reflected pressure bouncing phenomenon occurs due to a collision between the incident pressure and the reflected pressure, which causes the blast pressure to magnify, thereby increasing the ultimate pressure magnitude as well as the duration of the pressure. In turn, this causes greater damage to the structure compared with an external (unrestrained) blast (Stolz et al. 2013). If a blast occurs within a fully enclosed PCCV, recording of the data is nearly impossible because the blast destroys the gauges. Therefore, in this study, the internal blast was detonated inside a semi-open structure. This allowed a partial release of the internal blast pressure to control the damage to obtain accurate data. The blast pressure was released to the left and right open ends of the structure and measured with an incident pressure meter while the reflected pressure inside the structure was measured with a reflected pressure meter.

Damage assessments of PCCVs from explosion loading scenarios have been partially verified in previous studies (Choi et al. 2018). In this study, we evaluated the behavior of the outer wall of the PCCV in response to internal blast pressure loading. An internal blast loading scenario was selected in which an explosion occurred due to an unidentified explosive installation or failure of a mechanical device inside the PCCV. The average blast pressure (P_r) and the average unit impulse ($i_r/W^{1/3}$) were calculated based on standard TM5-1300 (UFC 3-340-02) from the US Army Corps of Engineers. The explosive pressure load was estimated from the data obtained from the experiment. Because the pressure bounced several times in the enclosed space, a level of pressure from the internal blast loading using an ANFO charge was selected so that only the pure blast pressure without debris would be applied. The ANFO weights of 22.68 kg (50 lbs), 24.95 kg (55 lbs), 27.22 kg, (60 lbs), 29.48 kg (65 lbs), and 31.75 kg (70 lbs) were used. For comparison, an RC structure of the same size was fabricated and blast tested using a charge of 22.68 kg (50 lbs).

Original target structure details

The test structures were modeled and designed based on a target structure of the Advanced Power Reactor 1400 (APR-1400) PCCV with a generation capacity of 1.4×10^6 kW, which was designed as a post-tensioned PSC structure with a service life of 60 years. The primary features of the structure were bi-directional prestressing (PS) tendons in the longitudinal and meridional directions in the wall and triple-directional PS tendons in the dome. The outer wall had three buttresses to anchor the unbonded tendons to allow partial overlapping at 240°. For the APR-1400 PCCV, the rebar and tendon ratios were 0.024 and 0.0107, respectively, giving a 10% higher PS force than in a conventional PCCV. The tubular structures were fabricated by scaling down the wall structure but applying the same reinforcement and tendon ratios as in the target structure.

Internal blast experiment

Test structure design and fabrication

Internal blast testing was performed with RC and PSC tubular structures modeled from a PCCV. It is important to note that this type of internal blast test had never previously been attempted. A total of six structures were tested using different internal blast charge weights comprising five PSC structures subjected to ANFO charges of 50, 55, 60, 65, and 70 lbs (PSC50, PSC55, PSC60, PSC65, and PSC70, respectively) and one RC structure subjected to a 50 lb charge (RC50). Both of the tubular RC and PSC structures were designed with outer and inner diameters of 2700 mm and 2000 mm, respectively. As shown in Fig. 1, the wall was 350 mm thick and 3600 mm long. The RC and PSC structures were designed with the same reinforcement ratio of 0.024. For the PSC structures, the PS tendon ratio of 0.0107 was applied to reflect a PCCV in service. The reason for using the same reinforcement ratio in the RC and the PSC structures was to understand the effect of PS force in the failure behavior of the PSC structures due to the PS confinement effect.

As shown in Fig. 1, D13 rebars were arranged in a grid pattern with a spacing of 100 mm and bi-directional PS tendons of 15.2 mm (SWPC 7B). The tendons had a yield strength of 1600 MPa, an ultimate strength of 1730 MPa, and a unit weight of 1.101 kg/m. As shown in Fig. 1*b*, the PS tendons were anchored at the buttress in 120° intervals with 240° interval lateral tendons partially overlapping each other to apply full continuity to the structure. The design PS force was 280 kN and a 1 mm strain gauge was attached to the mid-span of the tendon to check the effective PS force during PS work. The measurements showed that the PS forces applied varied 220–380 kN, even though the same PS force of 280 kN was applied to all of the structures. The variation probably came from the tests being conducted approximately 1–1.5 months from the initial application of the PS force, which induced slippage of the anchor and relaxation of the tendon strain. As expected, loss of the PS force was more significant in the meridional tendons than in the longitudinal tendons. The measurements of PS force, taken immediately after the PS work and just prior to the blast test, are summarized in Table 2. All of the structures were cast using concrete with a 28-day compressive strength of 40 MPa.

High strain rate compatible measurement system

The blast test was conducted at a test site operated by the Agency for Defense Development (ADD) in South Korea. As shown in Fig. 2, the supporting frame was constructed at a height of 1000 mm from the ground. The tubular structure, with a weight of 2600 kg, was

Fig. 1. Rebar, tendon, and structure details (unit: mm). [Colour online.]

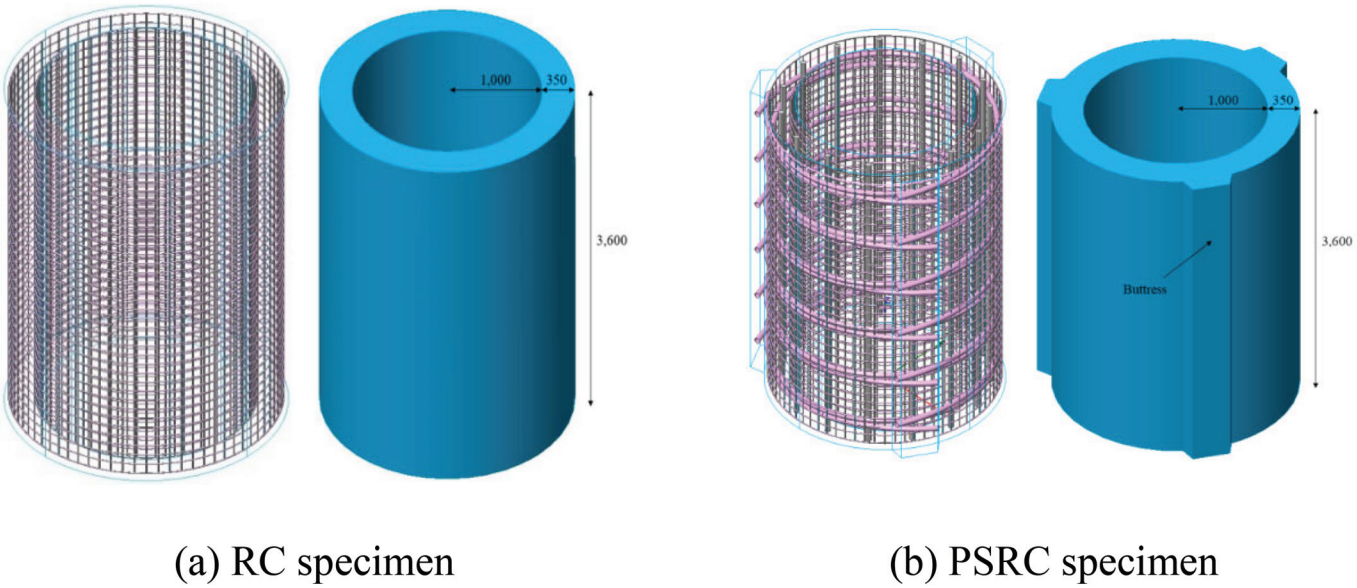

Fig. 2. Supporting frame. [Colour online.]

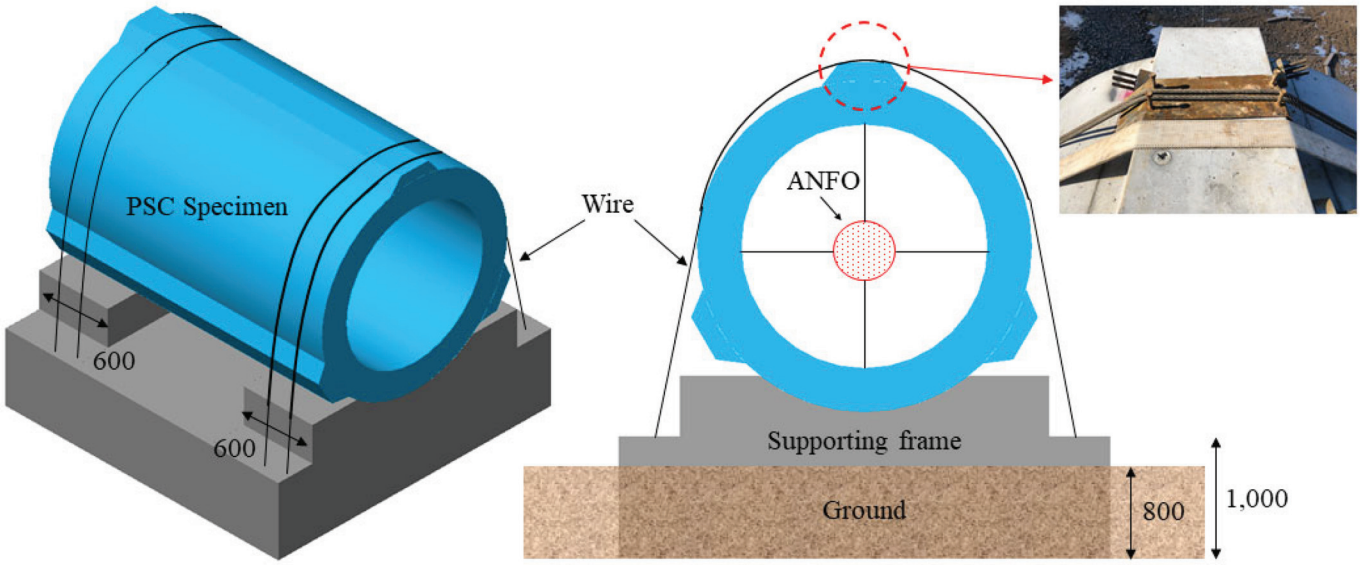

mounted on the support frame and tightened at both ends using a 100 mm wide flexible steel strap, chain block, and fastening buckle to maintain full fixture during the test. To conduct repeated tests at the site, the only feasible option with regard to the fixing the ends was the tie-down method. It is to be expected that there will be slight variability in the behavior due to the strong magnitude of the applied load with respect to the ends remaining in position. A rubber pad 10-mm thick was inserted between the structure and the support frame to prevent contact damage during the testing. A sensor jig was embedded in the mount so that the structure gauges remained in position throughout the testing. The setup for the structure test is shown schematically in Fig. 2. The strain gauges were attached to the support frame rebars and concrete to measure the strain of the support frames during the testing. The ANFO charge was placed at the center of the cross-section at the mid-span using four ties installed at 90° intervals to fix the charge in position.

Measurement system

Precise measurement of the behavior of the structure from the internal blast required instantaneous measuring equipment and data acquisition systems. Linear voltage displacement transformers (LVDTs), accelerometer, pressure meter, and a high-speed camera were used for the measurements. Figure 3 shows the locations of the embedded tendons and rebar gauges. The sensors were attached and embedded with the jigs during fabrication of the structure to keep them in position during the blast. The free-

Fig. 3. Locations and details of the strain and tendon gauges. [Colour online.]

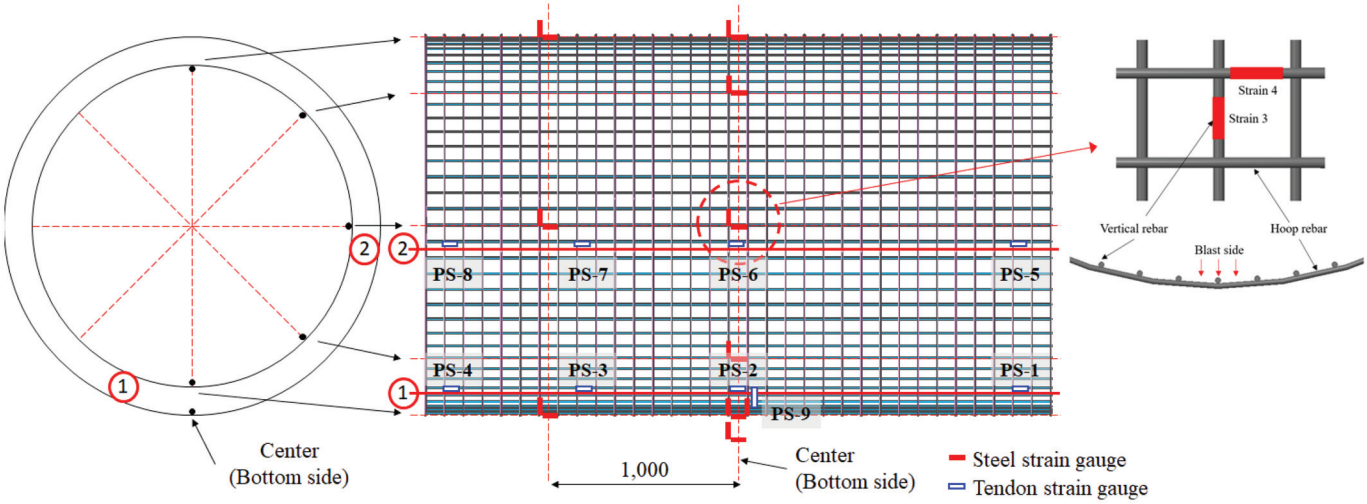

Fig. 4. (*a*) Internal blast test setup. (*b*) Sensor types and locations. [Colour online.]

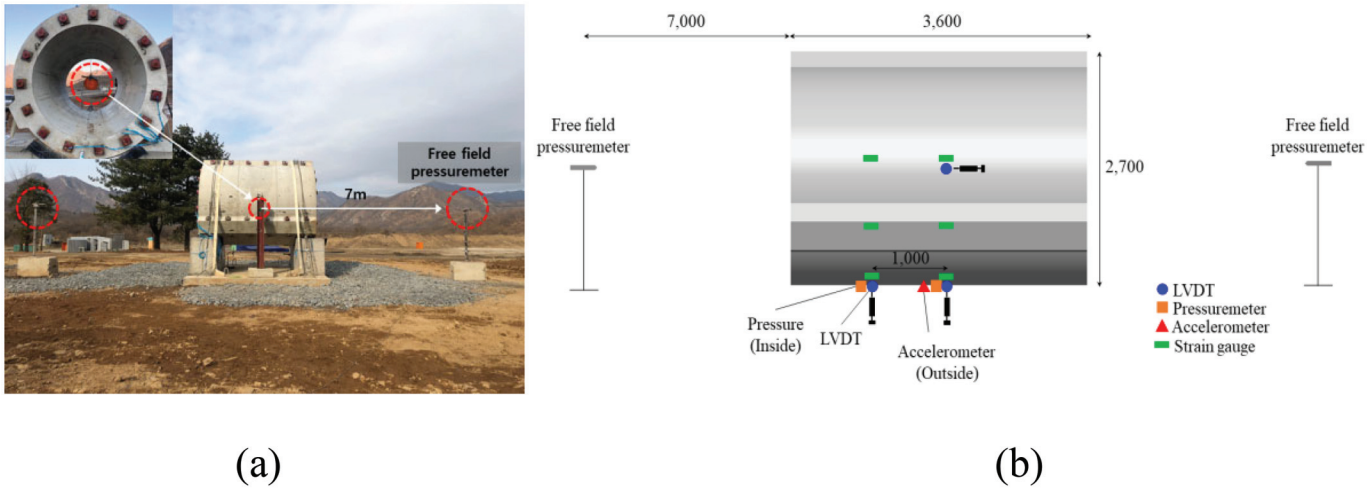

field incident pressure of the blast loading was measured using two 500 psi capacity instant pressure meters installed at 7000 mm from the left and right ends of the structure and placed at the same height as the blast charge. The reflected pressure of the internal blast was measured using the two-reflected pressure meters attached to the internal surface of the structure at the mid-span and 1000 mm from the mid-span. The maximum and residual deflections were measured from the exterior surface at the mid-span and 1000 mm from the mid-span using the ±100 mm spring-type dynamic LVDTs. An accelerometer with an allowable range of 50 000*g* was used on the external surface at the mid-span, which was the same location as the mid-span deflection measuring LVDT. In total, six concrete gauges were embedded at 1000 mm from the mid-span of the structure at 45° intervals. Nineteen rebar gauges were attached in the inner and outer rebars at the mid-span of the structure at 45° intervals in both longitudinal and meridional directions. Additionally, eight longitudinal tendon gauges were attached at the mid-span in 90° intervals. Figure 4 shows the details of the measurement gauge locations and types used in the test. The data logger used for data acquisition could sample signals at 200–500 kHz. Pressure, acceleration, and deflection were measured at 500 kHz and the strains in the rebar and concrete were measured at 200 kHz. For visual inspection of the internal blast pressure, video images of the blast were recorded using a high-speed camera (4000 frames/s).

Blast experiment modeling

Table 1 shows the free-field pressure, deflection, strain, and environmental conditions obtained from RC50, PSC50, PSC55, PSC60, PSC65, and PSC70. As shown in Table 1, when the weight of the blast charge increased, the magnitudes for all of the data increased. For example, when the weight of the explosive charge increased from 50 to 70 lbs, the peak incident pressure and duration increased from 0.2887 to 0.404 MPa and from 6.062 to 6.638 ms, respectively. The data for reflected pressure was only available for the RC50 and the PSC50, because all of the pressure

Table 1. Summary of the internal blast test data.

Value			RC50	PSC50	PSC55	PSC60	PSC65	PSC70
Free field pressure	Peak pressure (MPa)		0.317	0.289	0.344	0.375	0.386	0.404
	Duration (ms)		5.826	6.062	6.156	6.482	6.566	6.638
	Impulse (MPa/ms)		0.387	0.528	0.534	0.554	0.569	0.570
Deflection (mm)	Maximum	Mid-span (0°)	15.27	6.62	9.56	10.28	11.49	12.01
		Mid-span (90°)	4.76	3.80	4.49	8.49	4.60	9.63
		1000 mm	7.71	4.88	5.49	4.61	8.47	5.55
	Residual (mid-span 0°)		7.84	0.02	0.20	0.27	1.25	2.01
Strain ($\mu\varepsilon$)	Longitudinal rebar	Maximum	1476.31	526.24	783.44	903.86	939.93	1004.32
		Residual	228.23	–71.32	–10.07	–36.43	12.79	–111.87
	Lateral rebar	Maximum	20986.06	2615.22	2736.99	2934.85	3037.29	4857.67
		Residual	4813.75	–411.19	–85.13	152.17	–156.68	–242.27
	Concrete	Maximum	755.56	–245.08	–824.48	1284.74	–818.86	1517.03
		Residual	104.31	–48.29	–320.48	77.08	–204.18	141.77
	Tendon	Longitudinal	—	961.25	3429.96	3803.81	3938.99	6230.52
Environ. condition	Temperature (°C)		2.9	–5.1	–5.1	8.1	–4.3	–3.7
	Humidity (%)		16	34	34	33	30	35

Fig. 5. Energy release photos of for the 50 lb ANFO test (PSC50). [Colour online.]

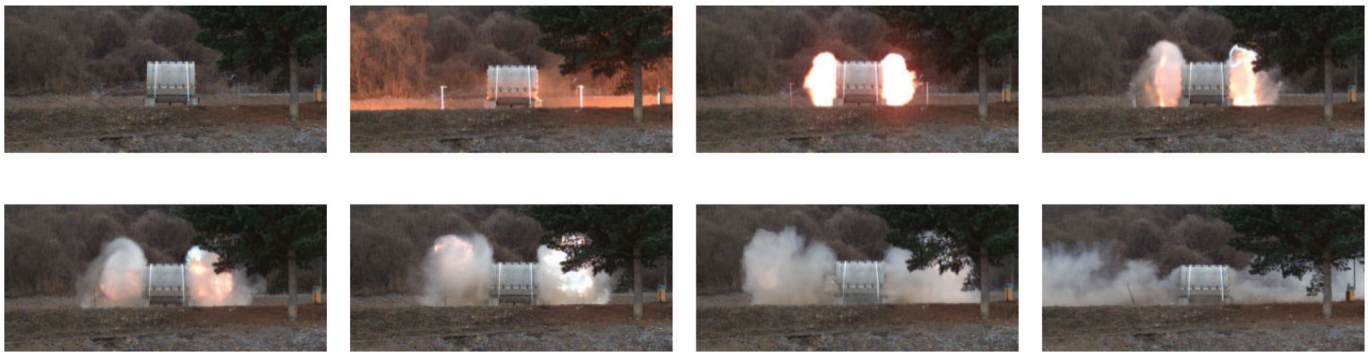

meters in the other structures were damaged. Therefore, Table 1 only includes the reflected pressure data for RC50 and PSC50.

Incident and reflected blast pressure

Figure 5 shows the high-speed camera photos that were taken of the internal blast test that was conducted with the 50 lb ANFO charge, which shows the blast pressure releasing through the left and right openings. Figure 6 compares the pressure data obtained from RC50 and PSC50 with the results calculated using ConWEP (U.S. Department of Defense 2002). Using ConWEP, only the first peak pressure load from the explosion was predicted. This study was conducted based on an internal blast with the dissipation of the blast pressure through the open ends. Because the test structure was semi-open and not a completely sealed structure as suggested by UFC 340, direct comparison with UFC 340 is not possible. Therefore, we assumed that the first peak pressure would be the maximum blast pressure applied to the inner surface, and used these data for all of our analyses.

Figures 6*a* and 6*b* show the free-field incident and internally reflected pressure, respectively, in relation to the time that the 50 lb ANFO charge was detonated, as measured with the pressure meter located 7000 mm from the mid-span under similar environmental conditions. For RC50 and PSC50, the peak pressure and impulse were 0.3166 MPa and 0.3874 MPa/ms, and 0.2887 MPa and 0.5280 MPa/ms, respectively. RC50 and PSC50 showed a very similar trend for incident pressure, but the impulse was 36.3% higher in PSC50 than in RC50. The incident peak pressure and impulse magnitude calculated by ConWEP were 0.2857 MPa and 0.3193 MPa/ms, respectively. The trend of the ConWEP-calculated incident pressure trend was similar to the test pressure, but the ConWEP impulse was 21.32% and 65.36% higher than in RC50 and PSC50, respectively. As shown in Fig. 6*b*, the reflected pressure was approximately 15 MPa higher in PSC50 than in RC50. The results also showed that there was a second peak after 10 ms from the reflected pressure, indicating the reflection of the blast pressure inside the structures. In the case of the free-field pressure measurements, all of the structures gave accurate results. However, for the measurements of internal reflected pressure, the proximity between the pressure sensors to the ANFO explosive charge inside the tube (500 mm) damaged the sensors. Also, because the reflected pressure was continuously bouncing off of the inner surface of the tube throughout the test, the sensors were damaged in several of the structures. Therefore, the reflected pressure data was only obtained from a limited number of structures. As shown in Figs. 6*a* and 6*b*, the time difference between the peak incident pressure and the reflected pressure between the test

Fig. 6. Blast pressure results for the 50 lb ANFO test. [Colour online.]

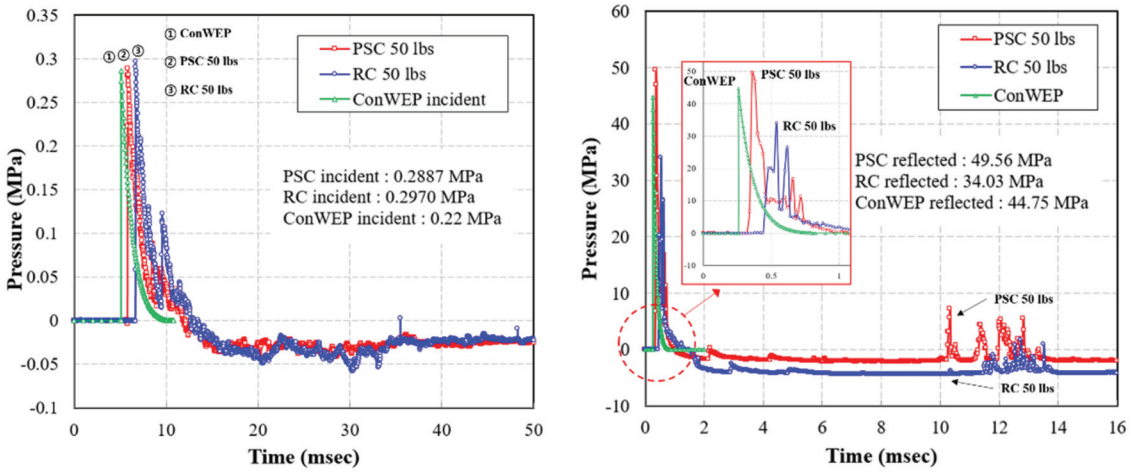

(a) Incident pressure (b) Reflected pressure

results and the ConWEP calculations were approximately 1.0 and 0.1 ms, respectively, which is probably because ConWEP is designed to calculate external blast pressure and does not consider environmental conditions such as the temperature, relative humidity, and wind speed in its calculations.

Prestressing tendon strain

Figure 7*a* shows the strain data for the PS tendons from internal blast loading. The peak strain for the PS tendon increased as the weight of the explosive charge increased. For PSC50, PSC60, and PSC70, the maximum strain results of the longitudinal tendon were 961.25, 3803.81, and 6230.52 με, respectively. The significant increase in the tendon strain was due to the increased internal blast load inducing plastic deformation in PSC60 and PSC70. Figures 7*b*–9*f* and Table 2 show the variation in PS force along the length of the structures during internal blast loading. Based on the effective PS force of 220–380 kN applied to the structures, there was a 60–100 kN decrease in the PS force because the anchors slipped and the tendon strain relaxed. In the longitudinal tendons (PS-1–PS-8), the PS force measured from the PS-2 tendon gauge at the bottom mid-span of PSC50, PSC55, PSC60, PSC65, and PSC70 increased by 10.09, 10.78, 16.31, 20.08, and 31.85 kN, respectively. The PS force measured at both ends of PS-1 and PS-4 increased slightly during the blast. Twenty-four hours after the test, the PS force for PSC50, PSC55, PSC60, PSC65, and PSC70 decreased by 5.96%, 6.38%, 10.47%, 12.06%, and 18.64%, respectively, indicating that the residual PS force was proportional to the plastic damage of the structures due to cracks and exfoliations.

Time-deflection relations

Deflection data in the PSC structures were measured from dynamic LVDTs installed at three locations on the external surface at the mid-span 0°, mid-span 90°, and 1000 mm from the mid-span 0°. For RC50 and PSC50, the maximum and residual deflections at the mid-span were 15.27 and 7.84 mm, and 6.62 and 0.02 mm, respectively. The maximum deflection and residual deflection for PSC50 were 56.65% and 99.74% less, respectively, than for RC50, owing to the greater structural stiffness due to the PS confinement effect. The deflection behavior was cyclic in both RC50 and PSC50 due to repeated application of the reflected pressures to the interior surface. The magnitude of deflection decreased over time in PSC50 owing to the restorative characteristics of the PSC member. However, as shown in Fig. 8*a*, the plastic deflection in RC50 due to blast pressure damaged the wall, resulting in a sudden drop in deflection after the initial peak deflection.

The maximum deflections of 6.62, 9.56, 10.28, 11.49, and 12.01 mm were measured in PSC50, PSC55, PSC60, PSC65, and PSC70, respectively. Comparison of the rates of maximum deflection for PSC55, PSC60, PSC65, and PSC70 with PSC50 indicated increases of 44.41%, 55.29%, 73.56%, and 81.42%, respectively. While the residual deflection for PSC50 was nearly zero, the values for PSC55, PSC60, PSC65, and PSC70 were 0.20, 0.27, 1.2, and 2.01 mm, respectively, indicating that the internal blast pressure induced plastic deformation in the structures. Further, the LVDT results showed greater mid-span deflection at the bottom surface (at the mid-span 0°) than at the side surface (90°) and 1000 mm away from the mid-span (0°), showing that gravity affected the dispersion of internal blast pressure.

Rebar and concrete strain

Figure 9 summarizes the strain data. Figure 9*a* shows the results of strain from the longitudinal rebar gauge attached to RC50 and PSC50. The maximum strain for RC50 was 1476.31 με, which was 2.84-times greater than the 526.24 με for PSC50. The residual strain for RC50 was 228.23 με, which was 3.2-times greater than the 71.32 με for PSC50. Figure 9*b* shows that the maximum strain in the lateral rebars for the RC50 and PSC50 were 20 986.06 and 2615.22 με, respectively. The maximum strain in the lateral rebar for the RC50 exceeded the yield strain, resulting in a maximum plastic strain of 4813.75 με. These results suggest that the strain in PSC50 was less than in RC50 due to the confinement effect of the bi-directional PSs. Figure 9*c* shows the strain data for the PSC with different ANFO charge weights. The maximum strains for the longitudinal rebars of the PSC55, PSC60, PSC65, and PSC70 were 783.44, 903.86, 939.93, and 1004.32 με, respectively, representing increases of approximately 148%, 171%, 179%, and 191%, respectively, compared with PSC50. The maximum strains on the lateral rebar for the PSC55, PSC60, PSC65, and PSC70 were 104%, 112%, 116%, and 186%, respectively, of that for PSC50, indicating that the increases in both the longitudinal and lateral rebar strains at the mid-span of the structures were proportional to the magnitude of the internal blast pressure. PSC70,

Fig. 7. Tendon strain and prestressed force variations. [Colour online.]

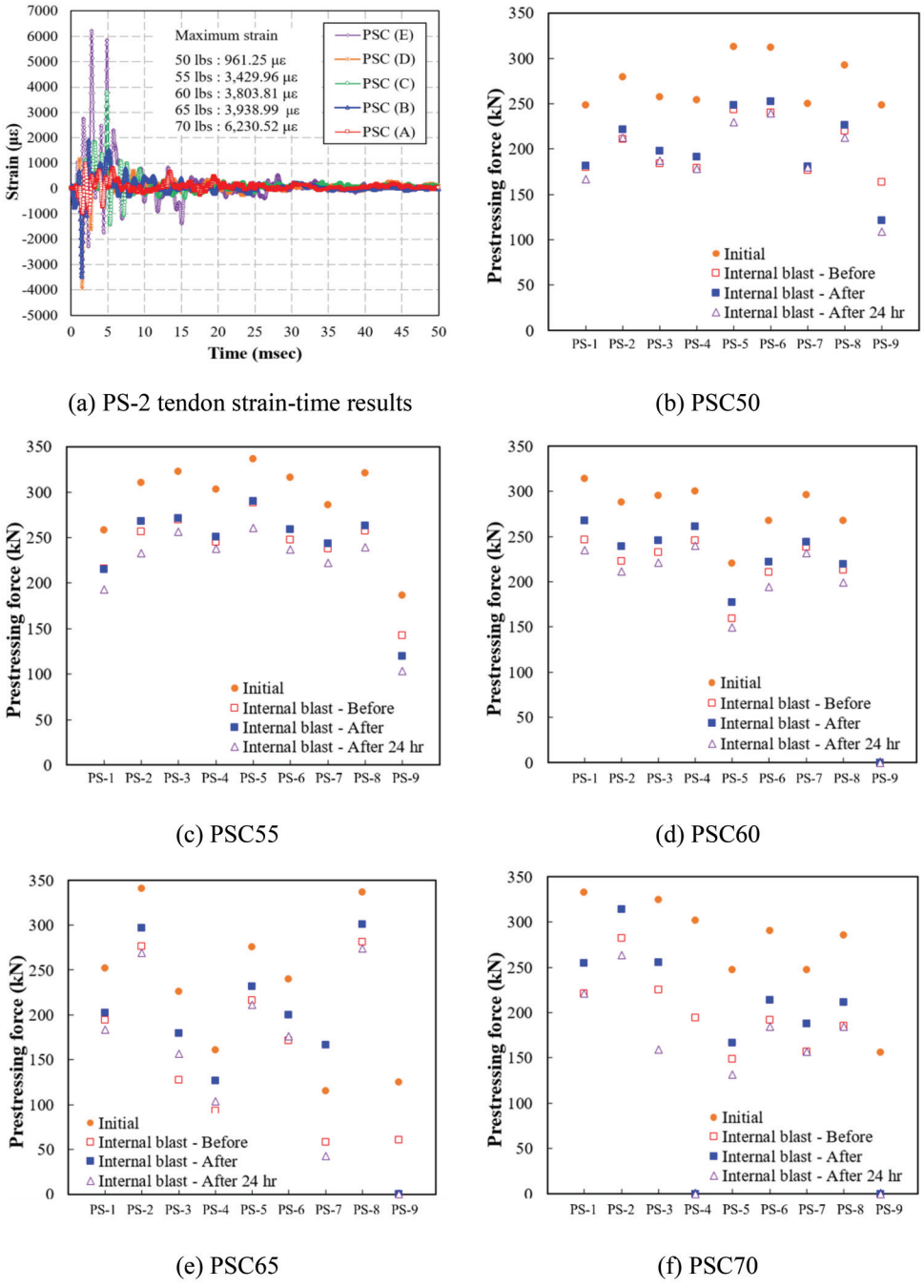

(a) PS-2 tendon strain-time results

(b) PSC50

(c) PSC55

(d) PSC60

(e) PSC65

(f) PSC70

which was subjected to the greatest explosive pressure, showed less strain than RC50, confirming the efficacy of increased wall stiffness due to PS at resisting blast pressure. For RC50 and PSC50, the maximum and residual strains observed in the concrete at the mid-span of the bottom structure were 755.56 and 104.31 με, and 245.08 and 48.29 με, respectively. The results were equivalent to a higher strain of 308% and 216%, respectively, in the RC50 compared with the PSC50, indicating a close relationship between the magnitude of the internal blast and the concrete strain and cracks. Our results also showed that there was significant strain-induced damage and cracks to the RC50 and PSC70 structures.

Crack patterns

Cracks were examined to determine the extent of damage to the structures. A comparison of the exterior surfaces of the RC50 and PSC50 showed that the PSC50 had fewer lateral cracks at the mid-span than the RC50 where the largest blast pressure was applied, while the left and right ends had minor longitudinal cracks. As shown in Fig. 10, RC50 had many lateral cracks that formed at the mid-span of the structure. RC50 had an even distribution of cracks across the top and bottom and left and right with significant macrocracks occurring in both the lateral and longitudinal directions at the mid-span. The pattern of cracks showed that the PSC had much better internal blast resistance

Table 2. Changes in prestressing force of the structure at the manufacturing stage and after the blast test.

	Initial prestress (manufacturing)		Release (before test)		Test (internal blast loading)		Release (after 24 h)	
Value	($\mu\varepsilon$)	(kN)	($\mu\varepsilon$)	(kN)	($\mu\varepsilon$)	(kN)	($\mu\varepsilon$)	(kN)
PSC50	2514	278.95	–613	210.94	91	221.03	–110	208.82
PSC55	3694	409.89	–53.04	356.85	–2	356.63	–23.86	332.77
PSC60	2594	287.83	–588	222.59	147	238.90	–246	211.60
PSC65	3975	441.01	–579	376.82	181	396.90	–253	368.83
PSC70	3448	382.59	–903	282.39	287	314.24	–460	263.20

Fig. 8. Time-deflection test results. [Colour online.]

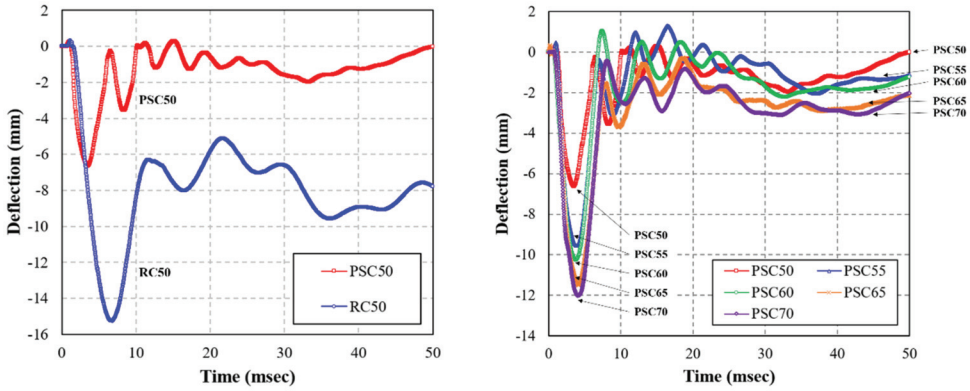

(a) RC50 and PSC50 (b) PSC specimens

than the RC50. PSC50 showed both longitudinal and lateral cracks, together with a lateral crack at the mid-span. Cracks were located primarily at the mid-span of the structure, with fewer cracks at the ends (e.g., the section fastened with a steel strap). For PSC60 and PSC70, the number of cracks increased as the charge weight increased. Lateral cracks were also observed at the mid-span of the PSC70. In both the RC and PSC structures, more cracks were found at the bottom than at other areas, probably due to the greatest pressure being applied toward the bottom of the structure as a result of gravity, although the charge was installed at the center of the cross-section with an equal standoff distance (1000 mm) from all sides.

Results and discussion

Analytical model of the structural stiffness modulus for PSC structures

Because a blast load applies a significant strain to a structure, the tensile stiffness of a blast-loaded structure will be totally different from a statically loaded structure. Therefore, the evaluation and analysis of dynamic tensile stiffness based on the experimental data should be performed. The calculation of tensile stiffness based on static behavior will not provide any meaningful information. As shown in Fig. 7, although the trends for maximum tendon strain in PSC50 and PSC55 were similar, PSC55 showed much greater tendon strain than PSC50, exceeding the range of the strain gauge. As shown in Fig. 8, the maximum deflection was much larger in PSC55 than in PSC50. Therefore, it was safe to assume that the structure subjected to the internal blast charge exceeding 50 lbs caused the structural tensile failure to occur when the structural stiffness could not resist the load, inducing plastic deformation. This assumption can be proven by the crack patterns discussed previously. The crack patterns in PSC50 and PSC55 were primarily lateral cracks; whereas, the crack patterns in PSC60 were both lateral and longitudinal. Based on these observations, the following equations were derived.

The wall stiffness (K) of the structure can be expressed by eq. 1 through the maximum internal blast force (F_{max}) and the maximum lateral wall deflection (u_{max}).

$$(1) \qquad F_{max} = K \cdot u_{max}$$

As shown in Fig. 11*a*, the majority of the internal blast pressure was primarily toward the left and right of the mid-span, equaling $2r_{internal}$ of 2000 mm at the instant when the maximum deflection occurred. Based on this assumption, the maximum deflection of the structure was selected from the measured deflection data between the maximum deflection at the mid-span or 1000 mm from the mid-span (eq. 2). As shown in Fig. 11*a*, $u_{mid\text{-}span}$ and u_{1000} were obtained from the dynamic LVDTs, which were installed at three locations on the external surface at the mid-span and 1000 mm from the mid-span during the blast test.

$$(2) \qquad u_{max} = \max(u_{mid-span} \text{ or } u_{1000})$$

If the majority of the applied pressure was ±1000 mm from the mid-span, then the maximum internal blast load F_{max} could be calculated by multiplying the internal surface area of the tube that experienced the majority of the pressure using the calculated maximum pressure (eq. 3):

$$(3) \qquad F_{max} = 2\pi r_{internal} \times 2000 \times P_{max}$$

where $r_{internal}$ is the internal radius of the circular cross-section of the structure, and 2000 mm is the span where the majority

Fig. 9. Strain test results. [Colour online.]

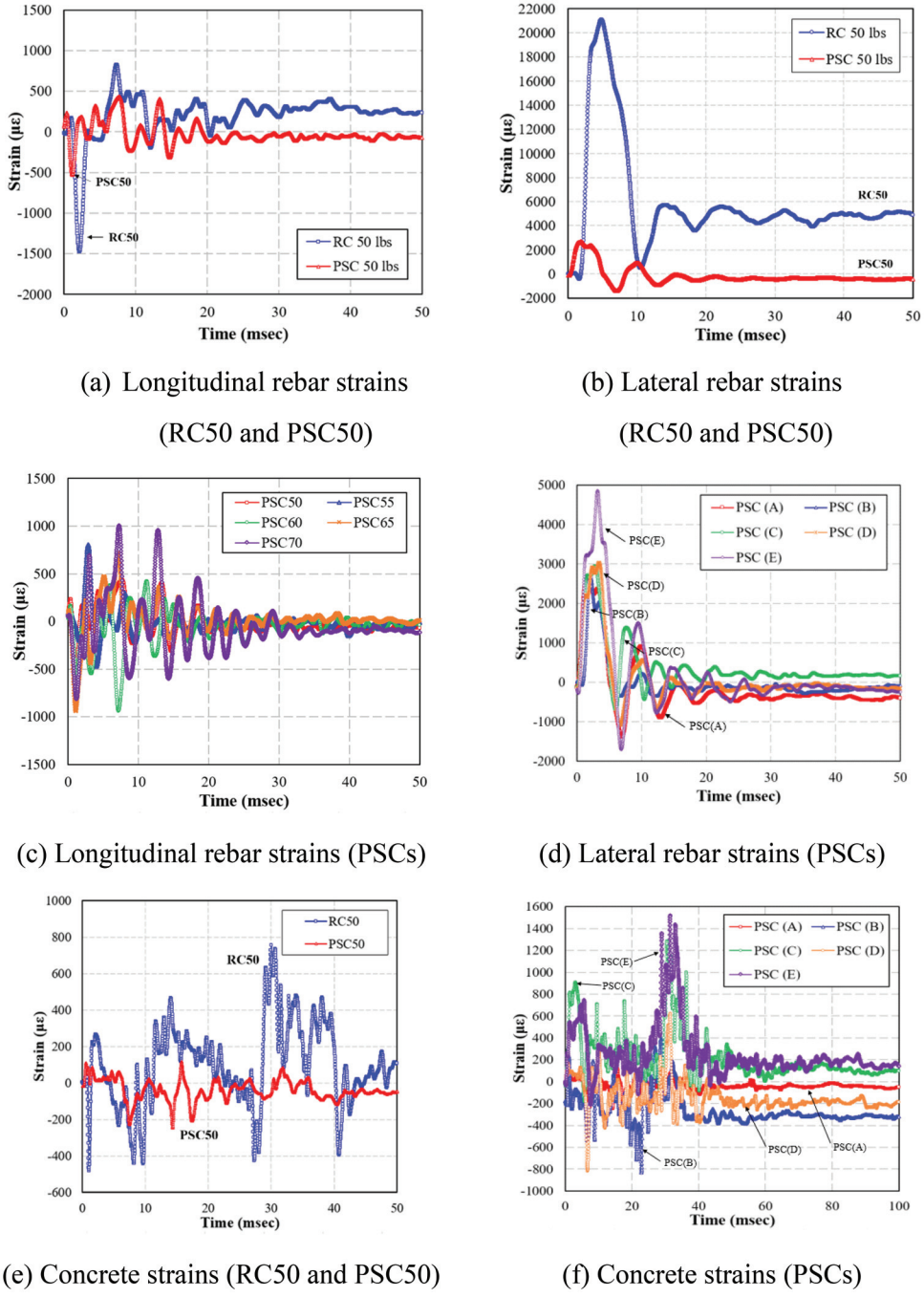

(a) Longitudinal rebar strains (RC50 and PSC50)

(b) Lateral rebar strains (RC50 and PSC50)

(c) Longitudinal rebar strains (PSCs)

(d) Lateral rebar strains (PSCs)

(e) Concrete strains (RC50 and PSC50)

(f) Concrete strains (PSCs)

of the internal blast pressure is applied. It is important to note that u_{max} comprises elastic and plastic deflections, as expressed in eq. 4. If there is a plastic deflection, then a maximum deflection would include both elastic and plastic deflections.

$$u_{max} = u_{el} + u_{pl} \quad (4)$$

where u_{el} is the maximum elastic deflection and u_{pl} is the plastic deflection. If eq. 4 is substituted into eq. 1, the applied force equation can be written as follows:

$$F_{max} = K(u_{el} + u_{pl}) = K_{el} \times u_{el} + K_{pl} \times u_{pl} \quad (5)$$

where the structural stiffness for elastic and plastic behavior is K_{el} and K_{pl}, respectively. Normally, it is nearly impossible to calculate or measure the structural stiffness coefficients of PSC members under blast loading. However, in this study, because the pressure and deflection of the PSC tubular members were measured from the test, K_{el} and K_{pl} could be obtained from the plot of F versus u test data. As shown in Fig. 12*a*, a drastic and distinct change to the slope of the curve was observed. The slope is the effective structural stiffness of the PSC tubular wall for internal blast loading. Up to PSC50, a linear elastic stiffness existed, followed by a semi-linear curve with a slightly varying slope from PSC50 to PSC70. The slightly varying slope between SPC50 and SPC70 resulted from the concrete cracking, changing the effects of the PS in the wall under blast loading. Therefore, the regression line with the optimal fit of the data was used to obtain the slope, which can be considered to be the

Fig. 10. Structural crack patterns. [Colour online.]

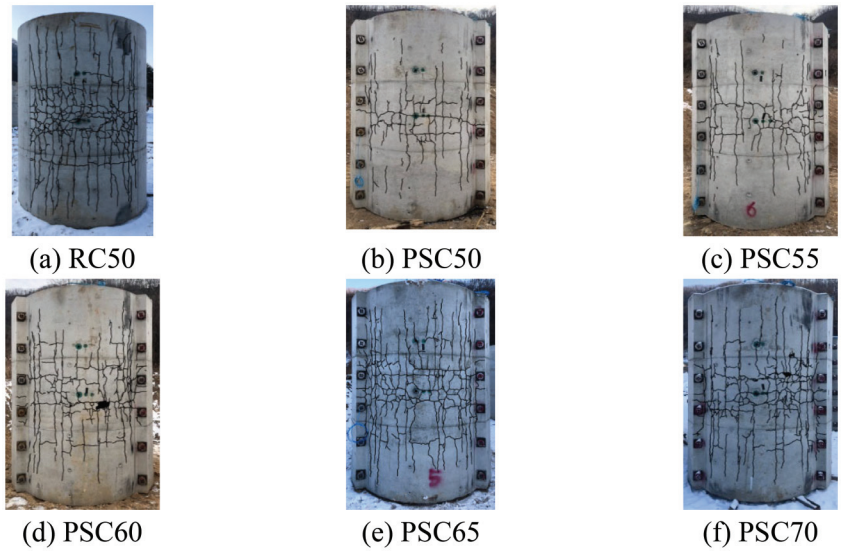

Fig. 11. Internal blast analytical models. [Colour online.]

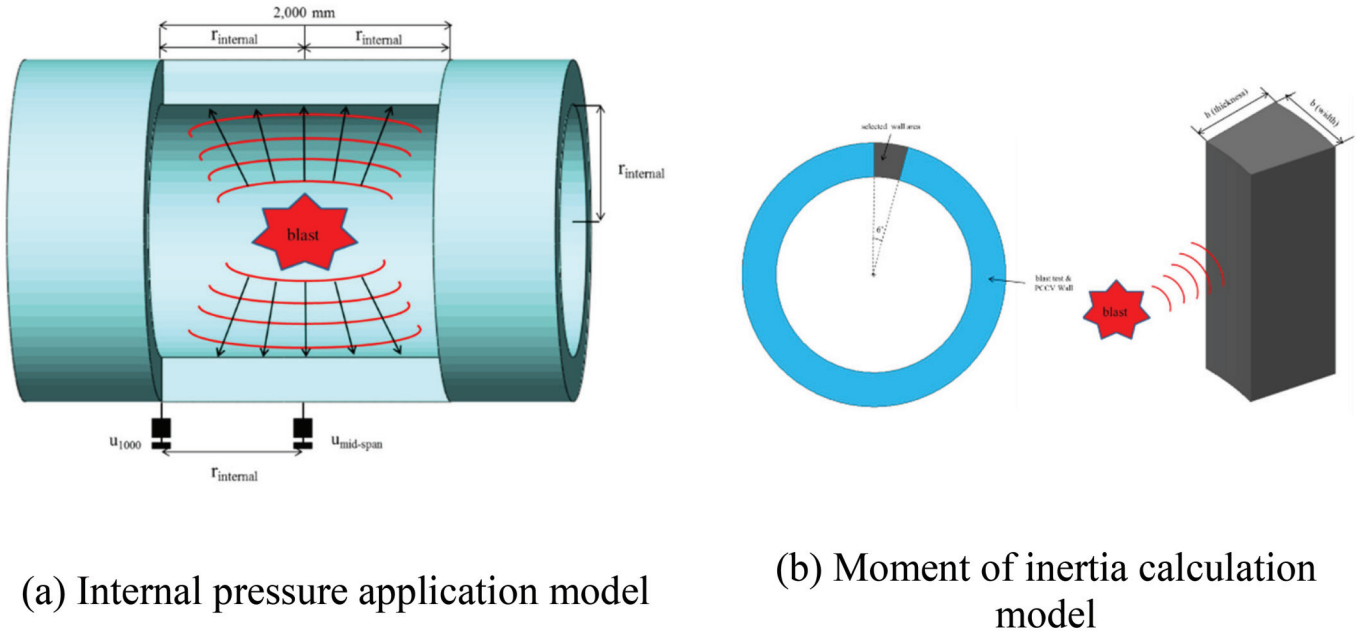

plastic stiffness of the wall. More specifically, from PSC50 to PSC60, stiffness decreased sharply and plastic behavior was observed. Between PSC60 and PSC70, the stiffness changed slightly but plastic deflection remained.

By obtaining the most effective elastic and plastic structural stiffness moduli of the PSC wall, the load-deflection behavior of the PSC tubular member could be predicted. Also, the ratio between the two stiffness moduli was used to calibrate the simulation program for the PSC tubular member, which was accomplished by increasing the internal blast pressure applied to the wall by multiplying it by the stiffness ratio (K_{el}:K_{pl}). This multiplication factor could also be used to reduce the initial PS force of the tendons by multiplying it with the stiffness ratio (K_{el}:K_{pl}) for a heavy blast charge (ANFO charge of 50 lbs).

Internal blast loading analysis using the simulation tool

Because a full-scale internal blast test on an actual PCCV was not feasible, it was necessary to develop a precise simulation tool to accurately assess the internal blast damage to a full-scale PCCV. In this study, the accuracy of the LS-DYNA simulation tool was improved by calibration with the experimental data. D13 rebar and the PS tendons were modeled as discrete beam elements embedded in 3D solid concrete (Fig. 13*a*). The layout and dimensions of the rebar and PS tendons were the same as those used in the experiments. The final boundary conditions at the same positions were used for all of the simulation cases, where the outer circumference of both ends was given a fixed condition as shown in Fig. 13*b*. For the concrete model, *MAT_CONCRETE_DAMAGE_REL3 (MAT_72R3) was used to consider the damage

Fig. 12. Elastic and plastic structural stiffness coefficient. [Colour online.]

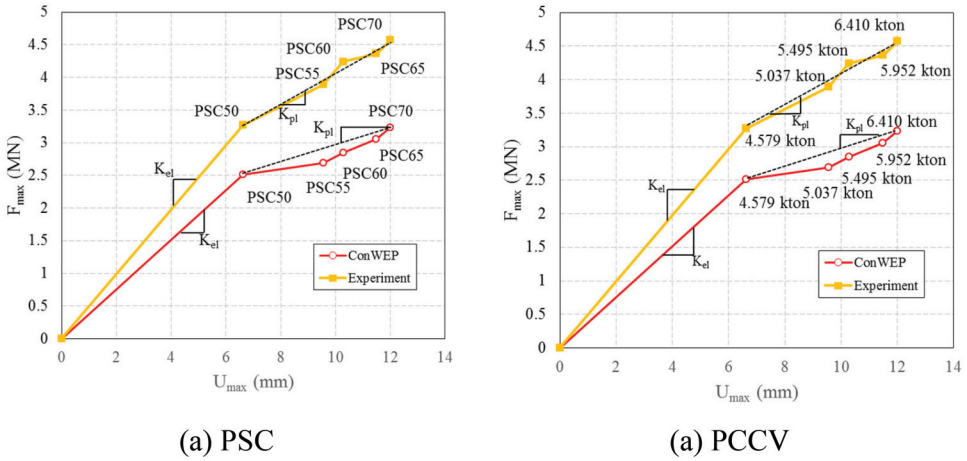

(a) PSC (a) PCCV

Fig. 13. Finite element model for LS-DYNA simulation. [Colour online.]

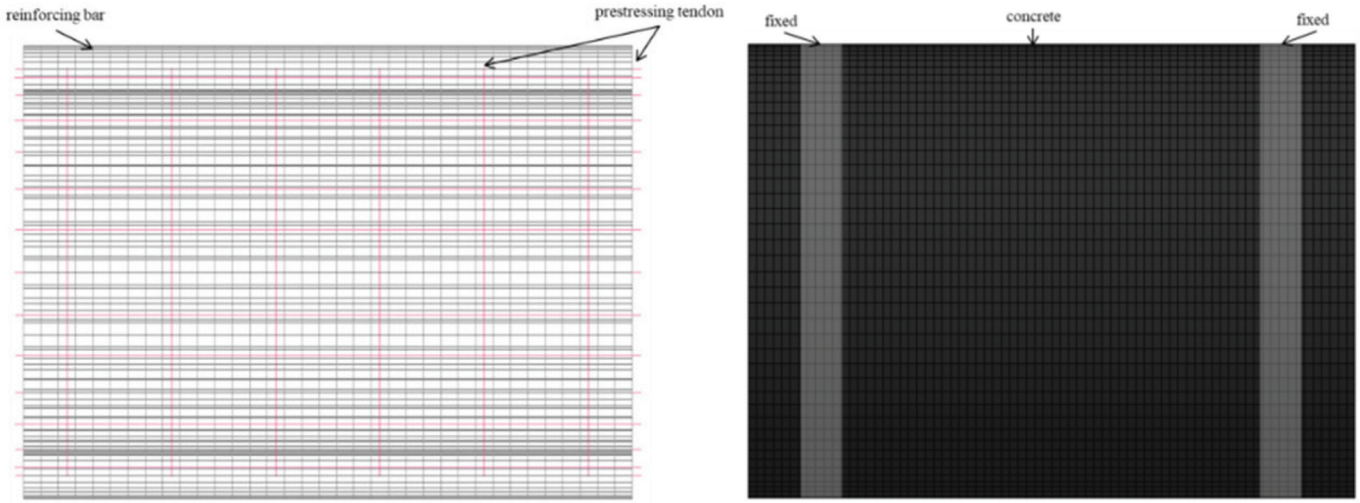

(a) Rebar and tendon modeling (b) Concrete and BC modeling

Fig. 14. Time-deflection results. [Colour online.]

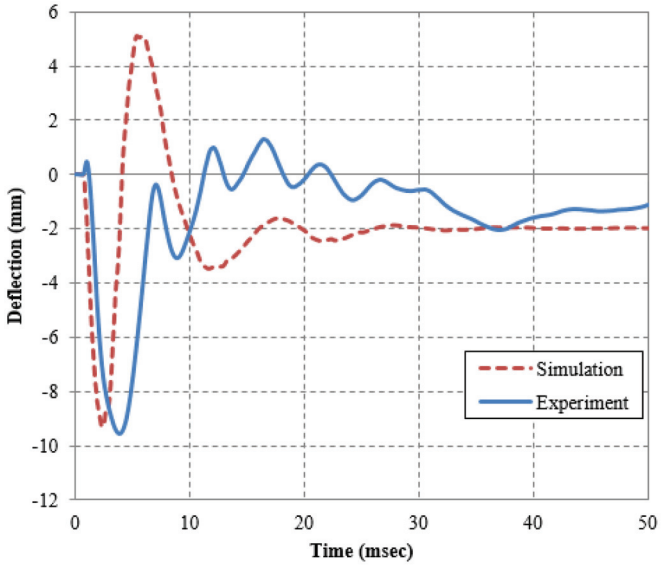

and strain rate. For the rebar model, *MAT_PIECEWISE_LINEAR_PLASTICITY (MAT_24) was used. PS was applied to a concrete member by temperature-induced shrinkage of the PS tendons (Jiang et al. 2015).

The maximum and residual deflection results from the blast simulations were compared with the results of the blasts in Fig. 14. For PSC55, the maximum and residual deflections from the simulation were 9.30 and 1.95 mm, respectively. The maximum and residual deflections from the test were 9.56 and 1.60 mm, respectively. The differences in maximum and residual deflections between the tests and the simulations of the PSC structures were 2.72% and 17.95%, respectively, owing to the differences in instantaneous loss of PS force and recovery in the tendons. Analysis of the simulation results indicated that the model has been sufficiently calibrated to be used for PCCV blast simulation.

Real-scale PCCV parametric analysis

Based on the results of the internal blast loading tests, structural stiffness for elasticity (K_{el}) and plasticity (K_{pl}) can be obtained as previously described. Using the structural stiffness obtained from the test, real-scale PCCV wall stiffness could be derived to predict the plastic deflection-inducing charge weight. The derivation of the full-scale PCCV was performed by calculating the difference between

Table 3. Correlating ANFO charge weight between the specimen and real prestressed concrete containment vessel (PCCV).

Member type	Correlating ANFO charge weight (lbs)				
PSC	50	55	60	65	70
PCCV wall	2 076 927 (4579 ton)	2 284 620 (5037 ton)	2 492 312 (5495 ton)	2 700 005 (5952 ton)	2 907 698 (6410 ton)

the modelled and the to-scale PSC wall. Generally, a moment of inertia (I) and a material elastic modulus (E) contribute to the structural stiffness of a member. Because all of the materials used in the model test were the same as for a full-scale PCCV, there was no difference in the material elastic modulus. Therefore, it was safe to assume that the difference in the moment of inertia of the model and the real PCCV wall would contribute to the structural stiffness. The moment of inertia of a member (I) was calculated using eq. 6.

$$I = \frac{bh^3}{12} \quad (6)$$

where b is the width of the section area and h is the height of the section area.

To correlate the member dimensions and calculate the moment of inertia for the PSC model and the to-scale PCCV wall, the dimensions were selected based on the assumptions shown in Fig. 11*b*. As shown in Fig. 11*b*, a cross-sectional angle of 6° was selected to obtain the width b and the thickness h. In this study, an APR-1400 PCCV was selected as the target structure for the parametric analysis. The internal diameter, wall thickness, and height of the real scale PCCV and test structure were 45 720, 1219, and 76 667 mm for the PCCV and 2700, 350, and 3600 mm for the test model. Based on the selection of 6°, the width and thickness of the PCCV and model used to calculate the moment of inertia become 45 720 and 1219 mm and 104.72 and 350 mm, respectively, denoted as b_{pccv} and h_{pccv} and b_{test}, and h_{test}, respectively. When the b_{pccv} and h_{pccv} and b_{test}, and h_{test} were substituted into eq. 6, the moment of inertia I_{pccv} and I_{test} were calculated as 1 391 309 886 009 and 33 494 413.78 mm^4, respectively. The ratio between I_{test} to I_{pccv} was approximately 1:41 538.54. Assuming that the moment of inertia (I) is proportional to the structural stiffness, K_{el} and K_{pl} for the PCCV wall were obtained from the F versus u graph as shown in Fig. 12*b*. Moreover, if the deflection of the PCCV wall was the same as that of the model wall according to internal blast loading was assumed, the explosive weights causing the deflections were proportional to the structural stiffness. Therefore, as shown in Table 3, the explosive weight required for a PCCV wall to fail was calculated as 41 538.54 times larger than that of the explosive test weight. As shown in Fig. 12*b*, with an explosive weight of up to 4.579 kt, the structure behaved elastically. From 4.579 to 6.410 kt, the structure behaved plastically. For the analysis, the slope between 4.579 and 6.410 kt was used as the plastic stiffness of the PCCV wall. By obtaining the elastic and plastic structural stiffness modulus of the PCCV wall, the load-deflection behavior of the PCCV wall could be predicted.

Conclusions

In this study, the internal blast resistance of PCCVs was evaluated by conducting an experiment on a scaled-down bi-directional PS concrete tubular PCCV structure. The test data obtained were used for the analysis to predict the minimum blast charge required to cause a PCCV of the type currently in service to fail.

1. The test data indicate that structural behavior is different for RC and PSC. Comparison of the results from ConWEP with our physical test results demonstrated that prediction of the pressure at varying distances from a blast source is possible.
2. The PSC structure showed greater damage as the weight of the ANFO charge increased. Nevertheless, the PSC structure was more effective than the RC structure at resisting internal blast loading because of the confinement effects due to PS.
3. Using our test data, the proposed analytical method can predict the blast charge weight required to cause internal failure of a to-scale PCCV.

Acknowledgements

This work was supported by a National Research Foundation of Korea (NRF) grant funded by the Korean government (MSIT: Ministry of Science and ICT) with the project numbers No. 2016R1A2B3009444 and No. 2017M2A8A4056624.

References

Choi, J.H., Choi, S.J., Kim, J.H.J., and Hong, K.N. 2018. Evaluation of blast resistance and failure behavior of prestressed concrete under blast loading. Construction and Building Materials, **173**: 550–572. doi:10.1016/j.conbuildmat.2018.04.047.

Hessheimer, M.F., Klamerus, E.W., Lambert, L.D., Rightley, G.S., and Dameron, R.A. 2003. Over-pressurization test of a 1:4-scale prestressed concrete containment vessel model (NUREG/CR-6810, SAND2003-0840P). U.S. Nuclear Regulatory Commission, Washington, DC.

Jiang, R.J., Kwong Au, F.T., and Xiao, Y.F. 2015. Prestressed concrete girder bridges with corrugated steel webs. Journal of Structural Engineering, ASCE, **141**(2): 04014108. doi:10.1061/(ASCE)ST.1943-541X.0001040.

Stolz, A., van Doormaal, A., Haberacker, C., Hüsken, G., Larcher, M., Saarenheimo, A., et al. 2013. Resistance of structures to explosion effects: review report of testing methods. Report EUR 26449 EN. Joint Research Centre, European Commission, Brussels, Belgium.

U.S. Department of Defense. 2002. Design and analysis of hardened structures to conventional weapons effects. UFC 3-340-01. U.S. Department of Defense, Washington, DC.

Yi, N.-H., Kim, J.-H.J., Han, T.-S., Cho, Y.-G., and Lee, J.-H. 2012. Blast-resistant characteristics of ultra-high strength concrete and reactive powder concrete. Construction and Building Materials, **28**(1): 694–707. doi:10.1016/j.conbuildmat.2011.09.014.